Association and diffusion of Li^+ in carboxymethylcellulose solutions with application to environmentally friendly Li-ion batteries: a combined Molecular Dynamics and NMR study

Mosè Casalegno,[b] Franca Castiglione,[b] Marco Passarello,[b] Andrea Mele,[c] Stefano Passerini[d,e] and Guido Raos*[a]

Abstract: Carboxymethylcellulose (CMC) has been proposed as a polymeric binder for the electrodes in environmentally friendly Li-ion batteries. Its physical properties and interaction with Li^+ ions in water are interesting from the point of view of electrode preparation—processability in water is one of the main reasons for its environmental friendliness—but also for its possible application in aqueous Li-ion batteries. We combine MD simulations and variable-time PFGSE-NMR spectroscopy to investigate Li^+ transport in CMC-based solutions. Both simulation and experiment show that, at concentrations such that Li-CMC has a gel like consistency, the Li^+ diffusion coefficient is still very close to that in water. These ions interact preferentially with CMC's carboxylate groups, giving rise to a rich variety of coordination patterns. However, the diffusion of Li^+ in these systems is essentially unrestricted, with a fast, nanosecond-scale exchange of the ions between CMC and the aqueous environment.

Introduction

The transition from fossil fuels to environmentally friendly and renewable energy sources is one of the foremost objectives of modern energy policies. Due to the intermittent nature of renewables, this requires the parallel development and large-scale deployment of adequate energy storage systems[1]. Among the various possible choices, electrochemical devices and in particular secondary batteries have received a great deal of attention, due to their capability to interconvert chemical and electrical energies with high efficiency and low environmental impact[2,3,4]. Compared to other types of batteries, Li-ion batteries (LIBs) possess higher energy density, higher output voltage per cell, and require lower maintenance[5,6]. Today LIBs are the main power source for portable electronic devices but, thanks to the above-mentioned advantages, they are being extensively researched also for applications such as electric and hybrid vehicles and large-scale stationary energy storage.[1,6] In order to meet the stringent requirements from the energy market, and taking into account the sheer scale of these newer applications, this research aims at improving the issues of safety, lifetime, cost, temperature operation range, materials availability and, last but not least, environmental friendliness.[7,8,9]

Early LIB architectures relied on a graphite anode, a lithium cobalt oxide cathode and an organic carbonate electrolyte, which are now being (slowly) replaced by safer — those LIBs were prone to catch fire due to thermal runway caused by reactions between the electrode materials and the electrolyte[10] — and more efficient ones. Major advances include the use of other transition metal oxides as cathodes (Co is a relatively rare and expensive element)[7,11], alloys and Si nanostructures as an alternative to graphite for the anodes[10] and polymeric binders[13], such as poly(vinylidenefluoride) (PVDF). Electronic and ion conduction phenomena within the electrodes, the electrolyte and at their interfaces are crucial in order to improve the charge-discharge rates and lifetime of the batteries[14,15]. An important, relatively new research trend concerns the use of water-based electrolyte media[16,17,18], as these would produce obvious advantages from the points of view of cost, safety and environmental friendliness. This requires the solutions of issues related to the stability of the electrolyte and the electrodes, but the use of highly concentrated "water-in-salt" media promotes the formation of a solid-electrolyte interphase layer which widens the electrochemical stability window[19]. The combination of an aqueous solution and a biomass-derived, polymeric gelling agent would be an ideal electrolyte from many points of view.[20-23] This emerges most clearly from the comparison with current Li-ion battery technologies. For example, the aqueous environment eliminates at the root the problem of flammability. It also eliminates the use volatile organic compounds, both as electrolyte media (the carbonates mentioned above) and as solvents in battery production, such as the toxic N-methylpyrrolidone used for PVDF-based systems. Finally, the natural polymer binder can be produced cheaply and abundantly by environmentally friendly chemical processes,[24] and does not pose special problems from a recycling perspective.

[a] Prof. Dr. G. Raos
Dipartimento di Chimica, Materiali e Ing. Chimica "G. Natta"
Politecnico di Milano,
Via L. Mancinelli 7, 20131 Milano, Italy
E-mail: guido.raos@polimi.it
[b] Dr. M. Casalegno, Dr. F. Castiglione, Dr. M. Passarello
Dipartimento di Chimica, Materiali e Ing. Chimica "G. Natta"
Politecnico di Milano,
Via L. Mancinelli 7, 20131 Milano, Italy
[c] Prof. Dr. A. Mele,
Dipartimento di Chimica, Materiali e Ing. Chimica "G. Natta"
Politecnico di Milano,
Piazza L. da Vinci, 32, 20133 Milano, Italy, and
CNR – ICRM
Via L. Mancinelli 7, 20131 Milano, Italy
[d] Prof. Dr. S. Passerini
Helmholtz Institute of Ulm (HIU),
Helmholtz Str.11, 89081, Ulm, Germany
[e] Karlsruhe Institute of Technology (KIT)
P.O.Box 3640, 76021 Karlsruhe, Germany

CMC is a linear polymeric derivative of cellulose with varying degrees of carboxymethyl substitution (DS)[26]. The molecular structure and numbering of its monomeric unit, as used in our simulations with DS=1, is shown in Figure 1. The ionic dissociation of the carboxymethyl groups to form carboxylate anions is responsible for the aqueous solubility of CMC, unlike cellulose which is insoluble. The counterions neutralizing their charge are typically Na^+ (CMC-Na) or Li^+ (CMC-Li). The use of CMC-Na as electrode binder already leads to good LIB performance[27,28], which is further improved by its replacement with CMC-Li[29]. This enhances the Li^+ content and prevents exchange reactions between sodium and lithium on the anode side. The excellent ion-conducting properties of CMC-Li mayrepresent a key advantage with respect to other polymeric binders. It has been suggested that these are due to CMC's ability to coordinate and transport the cations along or between adjacent chains[30]. However, the mechanism of lithium transport in CMC-Li (both aqueous solutions and the bulk, gel-like phase), which is of utmost importance for aqueous LIBs, has never been detailed at the molecular level. In general, it is necessary to understand the role of CMC in Li^+ transport, and the impact of CMC concentration on the Li diffusion coefficient.

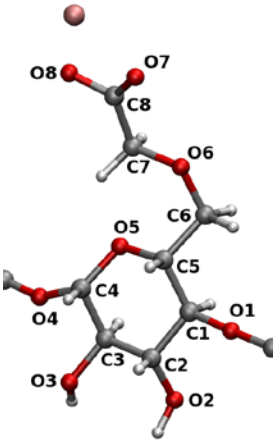

Figure 1. Structure of the CMC-Li monomer, with labeling of the oxygen (red) and carbon atoms (grey). The Li cation is also shown (pink).

In order to provide some background knowledge about these important aspects, in this work we characterize the structural and diffusive properties of Li^+ in CMC-Li/LiCl solutions. These model systems are relevant for the operation of water-based batteries. Combining ^{7}Li pulsed field gradient spin-echo (PFGSE) NMR measurements of Li^+ diffusion with Molecular Dynamics (MD) simulations, we show that, in comparison to solutions with the same ionic strength, CMC produces a modest reduction of the Li^+ diffusion coefficient. Analysis of the MD trajectories provides an interpretation of this effect in terms of fast association equilibria between Li^+ and CMC. These findings and their implications are discussed in relation to the development of environmentally friendly LIBs employing water-based electrolytes.

Results and Discussion

NMR results. The motion experienced by Li ions in the examined systems can be studied experimentally by PFGSE-NMR spectroscopy. This methodology has been successfully applied to the diffusions of solutes within polymeric matrices [31]. It involves the measurement at variable times of the Li ion mean-square displacement along the z axis (MSD or $\overline{z^2}$, where *z* is the direction of application of the pulsed field gradients). The main steps can be outlined as follows:

i) The MSD for each observation time Δ is obtained by fitting the gradient-dependent NMR signal intensities $I(q,t_d)$ according to the equation:

$$I(q,t_d) = I_0 \exp\left(-\frac{1}{2}q^2\overline{z^2}(t_d)\right) \quad (1)$$

Here I_0 is the echo intensity without field gradient, $t_d = \Delta - \delta/3$ is the diffusion time and $q=\gamma\delta g$, where γ is the magnetogyric ratio of the observed nucleus, g is the field gradient and δ is an instrumental time variable (see the Experimental Section).

ii) The MSD is related to the diffusion time t_d according to:

$$\overline{z^2}(t_d) = 2Dt_d^{\alpha} \quad (2)$$

The α exponent defines the type of motion: $\alpha \neq 1$ indicates non-Gaussian motion, as often observed in heterogeneous and confined systems[32]. In particular, superdiffusive and subdiffusive regimes correspond to $\alpha>1$ and $\alpha<1$, respectively. Conversely, $\alpha=1$ indicates unrestricted Gaussian motion, as commonly observed in isotropic liquid solutions. The α exponent can be determined by a linear fit of a log-log plot of the MSD *vs* t_d.

iii) In the Gaussian case, Eq. (1) turns into the well known Stejskal-Tanner equation:

$$I(q,t_d) = I_0 \exp\left[-q^2 D t_d\right] \quad (3)$$

so that Dt_d can be obtained from eq. (3) by a linear regression of $\ln(I/I_0)$ *vs* q^2.

This protocol has been applied to two aqueous LiCl solutions (SOL15 and SOL40, in order of decreasing concentration) and to three CMC-containing gels (CMC15, CMC25 and CMC40, also in order of decreasing concentration: see the Experimental Section for details). Figure 2a gives, as an example, the normalized experimental signal decays $I(q,t_d)$ in CMC15, plotted on a semilogarithmic scale against q^2 for the set of used diffusion times Δ=100–300 ms. The slopes of the linear fits provide the MSD values for each Δ value. The log-log plot of the MSD *vs* t_d is reported in Figure 2b. In all cases the α exponent was found to be 1.00, giving evidence that Li^+ ions experience the same pure unrestricted Gaussian motion in the water solutions and in the CMC-based gels. This finding is surprising, given the high viscosity of CMC containing systems.

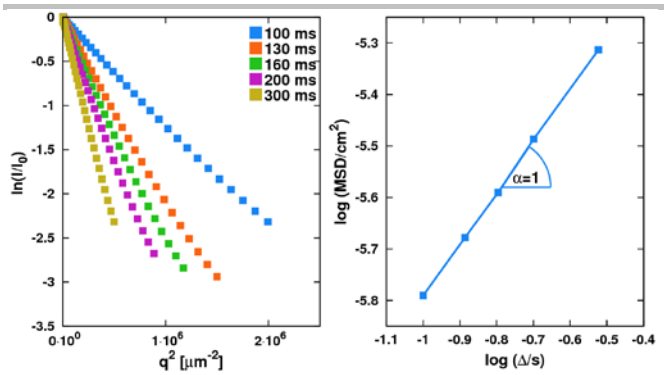

Fig. 2. PFGSE-NMR results for sample CMC15. Panel a) normalized NMR signal decay *ln(I/I$_0$) versus q*^{2}. Panel b) log-log plot of the MSD *versus* diffusion time.

The experimental diffusion coefficients *D* determined for all samples at 305 K are reported in Table 1, alongside the simulation results. These will be compared and discussed in the "MD results: dynamics" subsection. But first, we examine the molecular interactions and equilibrium structural properties emerging from the MD simulations.

Table 1. Experimental and calculated diffusion coefficients of Li^+ in the investigated systems.

System	D_{exp} (cm^2/s)	D_{calc} (cm^2/s)	D_{calc}/D_{exp}
SOL40	$1.03(\pm0.01)\times10^{-5}$	$1.60(\pm0.06)\times10^{-5}$	1.55
SOL15	$0.94(\pm0.01)\times10^{-5}$	$1.07(\pm0.08)\times10^{-5}$	1.14
CMC40	$0.92(\pm0.02)\times10^{-5}$	$1.18(\pm0.03)\times10^{-5}$	1.28
CMC25	$0.88(\pm0.02)\times10^{-5}$	$0.91(\pm0.03)\times10^{-5}$	1.03
CMC15	$0.82(\pm0.02)\times10^{-5}$	$0.78(\pm0.03)\times10^{-5}$	0.96

MD results: structure. As explained in the Experimental Section, we carried out MD simulation on three CMC-Li/LiCl systems at concentrations comparable to the experimental ones (CMC15, CMC25 and CMC40, where the former has the highest CMC concentration), and on two CMC-free LiCl solution (SOL40 and SOL15). The results for the intermediate composition (CMC25) are generally consistent with the two extreme ones (CMC40 and CMC25), therefore in the following discussion we mostly focus on the latter.

The equilibrium distribution of the Li^+ cations around CMC's and water's oxygen atoms has been characterized by means of pairwise radial distribution functions (RDFs). These count the average number of times than two types of atoms are found at a distance *r*, and normalize it by the value expected for an uncorrelated system of non-interacting atoms, at the same number density. Following common practice, they are denoted by $g_{XY}(r)$, where X and Y are the chemical identities of the atoms involved in the distribution.

Fig. 3 shows the lithium-oxygen pairwise distributions for the CMC15 and CMC40 systems ($g_{Li,OX}(r)$, where OX is the oxygen type). The oxygen atoms have been grouped into: carboxyl oxygen in CMC (OC), oxygen bonded to the carboxymethyl groups within CMC's side chains (OM), oxygen belonging to CMC's backbone (there are five of them for each monomer, and we denote them collectively by OB) and water oxygen (OW). The RDFs for the two systems do not show major, unexpected differences. Peak positions and intensities are slightly affected by dilution, but these small differences are often difficult to appreciate by visual inspection.

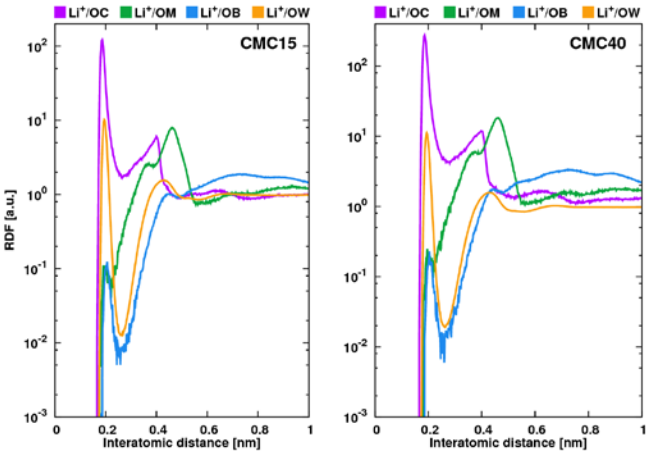

Fig. 3. Lithium-Oxygen RDFs for CMC15 and CMC40. Oxygen atoms are assigned to different classes, as discussed in the main text.

The most outstanding and relevant pair distribution functions are the ones for the carbonyl oxygen. The Li^+/OC distributions in Fig. 3 have a very strong and sharp peak at about 0.19 nm, whose height is one order of magnitude larger than the corresponding one for Li^+/OW. This indicates the formation of tight ion pairs. This is reasonable, considering the net negative charge on the carboxylate group. The Li^+/OC distribution has also a secondary, much broader peak at about 0.40 nm. This can be interpreted on geometrical grounds since, whenever one lithium cation is closely associated with one carboxyl oxygen, by necessity there will be a second oxygen belonging to the same carboxyl group slightly farther away. The broadness of the second peak is due to the conformational freedom of the carboxyl group around the C-C bond, which allows a variety of Li^+/OC coordination modes (see below).

The RDF for Li^+/OM shows a peak at 0.46 nm. This does not correspond to a strong and direct interaction between these atoms but, like the second peak of Li^+/OC, it mainly reflects the proximity to a strongly interacting Li-carboxylate ion pair. The Li^+/OB distribution has virtually no significant features, if we mean by this the presence of short-range peaks with values appreciably greater than unity. The RDF describing water oxygen distribution around Li^+ is characterized by a sharp maximum at about 0.2 nm and another one around 0.4 nm, corresponding to the water molecules forming the first and second solvation shells around the cations.

Integration of these RDFs up to an upper cutoff *R* gives the coordination numbers of the Li ions, according to the equation:

$$C_{Li}^{OX}(R) = 4\pi n_{OX} \int_0^R g_{Li,OX}(r) r^2 dr \qquad (4)$$

where n_{OX} is the number density of oxygen atoms of a given type. Therefore C_{Li}^{OC}, C_{Li}^{OM}, C_{Li}^{OB} and C_{Li}^{OW} count the average number of carbonyl, carboxymethyl, backbone and water oxygen atoms surrounding a Li^+ ion. Note that, while we always have

$g_{XY}(r)=g_{YX}(r)$, the same is not true for the coordination numbers: in general $C_X^Y(R) \neq C_Y^X(R)$.

Table 2. Coordination numbers of the Li^+, calculated with the distance cutoff R=0.256 nm. The oxygen types (OC, OM, OB and OW) have been defined in the main text.

System	OC	OM	OB	OW
CMC15	0.367	0.00078	0.00116	2.944
CMC40	0.317	0.00063	0.00073	3.297
SOL15	-	-	-	3.158

The results in Table 2 have been calculated using the upper cutoff R=0.256 nm, corresponding to the first minimum after the main peak of the Li^+/OC RDF. These coordination numbers confirm that a Li^+ ion has a strong tendency to be surrounded by water—obvious, since this is by far the majority component in our systems—but it also has an appreciable probability to interact with the carboxylate groups. Their interaction with CMC's methoxy and backbone oxygens is almost negligible.

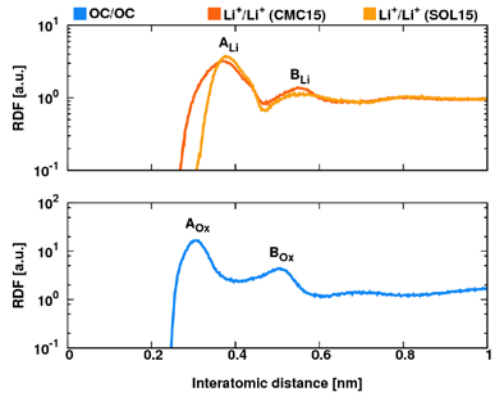

Fig.4. Top panel: Li^+/Li^+ RDFs for CMC15 and SOL15. Bottom panel: OC/OC RDF for CMC15

According to the previous discussion, it is also interesting to calculate the average extent of neutralization of CMC's negative charges by the metal ions. We may obtain it from the number of Li^+ within a distance R from a carboxylate oxygen (OC). This is given by a formula analogous to Eq. (4), with n_{Li} in place of n_{OC}. Thus the two coordination numbers are simply related by:

$$C_{OC}^{Li}(R) = \frac{n_{Li}}{n_{OC}} C_{Li}^{OC}(R) \qquad (5)$$

In our systems $n_{Li}/n_{OC}=2.5$. Combining this with the data in Table 2, we obtain 0.915 in CMC15 and 0.792 in CMC40. Finally, remembering that there are two of such oxygen atoms within a carboxylate group, the average number of closely associated Li^+ ions per carboxylate is 1.83 in CMC15 and 1.58 in CMC40. This does not imply a true charge inversion[33], which is typically associated with the presence of multi-valent counterions, because the previous analysis is based on a single distance cutoff and does not take into account the distribution of the negative chloride ions.

Fig. 4 shows the Li^+/Li^+ and OC/OC pairwise distributions (for clarity, the short-range peak associated with geminal carboxyl oxygens has been omitted from the latter). In the Li^+/Li^+ RDF, two major peaks can be distinguished at about 0.38 and 0.55 nm (A_{Li} and B_{Li}, respectively). These maxima are similar but not exactly superimposable to those observed in water (SOL15). In particular, the interaction between Li^+ and CMC broadens and shifts the A_{Li} peak toward shorter distances. The two peaks in the OC/OC RDF, centered at 0.30 and 0.51 nm (A_{Ox} and B_{Ox}, respectively), provide a clear indication for the existence of molecular conformations characterized by an association of two or more carboxyl groups. These peculiar features of these RDFs are related, as illustrated by Figure 5, which shows a short portion of a CMC oligomer extracted from a snapshot of the MD simulation of the CMC15 system. The contributions to the A_{Li}, B_{Li}, A_{Ox} and B_{Ox} peaks have been highlighted. Clearly, the short-range Li^+/Li^+ interactions are mediated by a carboxyl group. Other snapshots (not shown) demonstrate that the opposite is also possible, with Li^+ mediating carboxyl/carboxyl interactions. To appreciate their real importance, it is necessary to perform a quantitative analysis of the possible Li^+/carboxylate coordination patterns

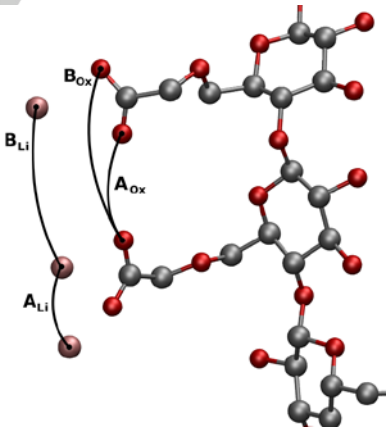

Fig. 5. Portion of a single CMC-Li oligomer extracted from an MD snapshot (CMC15 system), showing the interactions between Li+ and carboxyl groups. Contributions to the A_{Li}, B_{Li}, A_{Ox} and B_{Ox} peaks, as defined in Fig. 4, have been highlighted.

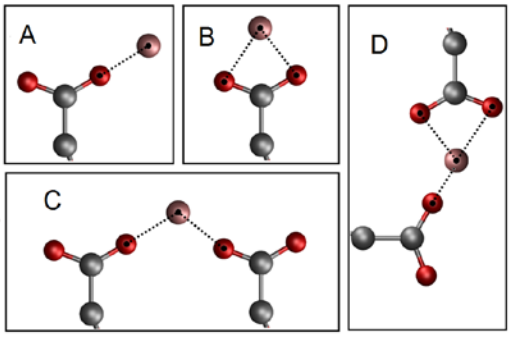

Fig. 6. Main coordination patterns of Li^+ with one OC (A), two OC belonging to different (B) or the same (C) carboxyl units, three OC belonging to two carboxyl groups (D). See Table 3 for the other patterns.

The analysis of the distribution of carboxylates around the cations reveals a rich variety of coordination patterns, with Li^+

interacting with variable number of oxygens belonging to one, two, or even three carboxyl units. The occurrence of each situation is given in Table 3 (error bars are of the order of 1%, for the most abundant situations). For simplicity, these have been derived considering intramolecular coordinations, with all the carboxyls belonging to the same oligomer. The most abundant patterns are also represented graphically in Figure 6.

Table 3. Definition and percentages of occurrence of the lithium-carboxyl coordination patterns in the CMC15 and CMC40 systems.

Pattern	N. of OC	N. carboxyl units	CMC15	CMC40
A	1	1	62.9%	48.7%
B	2	1	15.4%	16.5%
C	2	2	13.1%	20.9%
D	3	2	5.9%	10.0%
E	4	2	0.4%	0.5%
F	3	3	1.4%	2.0%
G	4	3	0.1%	1.3%

Pattern A is associated with the interaction between Li^+ and one, single carboxyl oxygen. Its percentage is 63% in CMC15, 49% in CMC40. The occurrence of pattern B, involving the coordination of Li^+ with two oxygens on the same carboxyl unit, reaches similar values in both systems (roughly 15%). A Li^+ may also bridge two carboxyl groups, and this mostly occurs via patterns C and D. The sum of their overall populations is 19% in CMC15 and 31% in CMC40. Note that the two carboxyl groups may belong both to adjacent and, to a smaller degree, also non-adjacent monomers. The formation of these intramolecular bridge patterns is consistent with the OC-OC and Li-OC RDFs discussed previously and points to the possibility of conformational changes in CMC chains, depending on their concentration and that of the added Li salt.

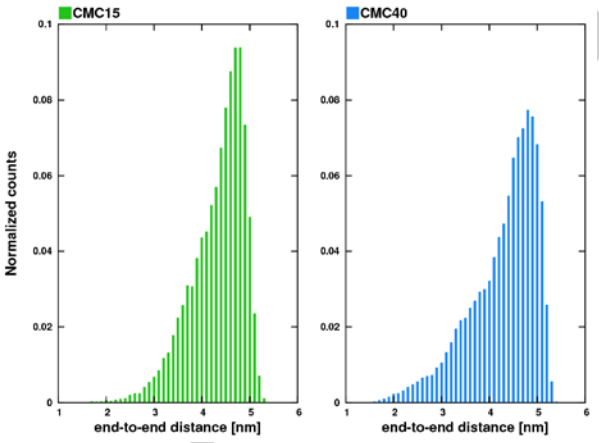

Fig. 7. Distributions of the oligomers' end-to-end distances in CMC15 and CMC40.

Fig. 7 shows the normalized distributions of the end-to-end distances, measured between the terminal methoxy groups of the CMC oligomers. The root-mean-square values are rather similar, namely 4.34 nm CMC15 and 4.38 nm in CMC40. However the latter shows a broader distribution, with a somewhat higher population of compact conformations. The difference between these distributions can be rationalized on the basis of the Li^+/OC coordination discussed above. The high percentage of bridge configurations (patterns C and D) in CMC40 apparently produces conformations characterized by shorter end-to-end distances. These differences appear to be relatively small in our simulations employing short oligomers, but they may be much more significant in high molar mass CMC polymers. Indeed, the average degree of polymerization of our experimental CMC samples is estimated to be of the order 10^3 glucose units, roughly 100 times larger than in our computational model. MD simulations for such high molar masses are presently unfeasible. Nonetheless, it is well known from polymer physics that the overall size of long, flexible chain molecules is controlled by scaling laws which can produce large amplifications of small, local conformational changes (see ref. 31b, for example).

MD results: dynamics. We now turn to the discussion of the diffusion and, more generally, the dynamics of Li^+ and CMC in water. Understanding and controlling these properties is essential for the development of better aqueous Li-ion batteries. Table 1 compares the NMR results with those obtained from the MSDs recorded during the MD simulations:

$$D = \lim_{\tau \to \infty} \frac{\left\langle \left[\mathbf{r}_i(t+\tau) - \mathbf{r}_i(t) \right]^2 \right\rangle}{6\tau} \qquad (6)$$

where the angular angular brackets indicate an average over all lithium ions *i* and all time origins *t*. Despite the differences between the experimental samples and our model systems (MW and DS of CMC, for example), we find good agreement between the calculated and experimental quantities. The simulated Li^+ diffusion coefficients are typically within 20% from the experimental ones. Considering the approximation in our model, such as the use of a non-polarizable force field, this is quite satisfactory. The fact that the only noteworthy discrepancy between simulation and experiment occurs in the most dilute aqueous solution (SOL40), while there is almost perfect agreement for the most "difficult" cases (CMC25 and CM15), indicates that here there might well be a partial cancellation of errors.

Overall, the simulations reproduce two important trends: the addition of CMC to the aqueous electrolyte solution produces a modest reduction of the Li^+ diffusivity (compare SOL15 and CMC15, or SOL40 and CMC40), while diluting the CMC solution increases it slightly (compare CMC15, CMC25 and CMC40).

Having validated the MD simulations against the experimental data, we may use them to extract further mechanistic details about the Li^+ dynamics. The Van Hove self-correlation function[34], $G_s(r,\tau)$, can be used to probe the dynamics of a single particle in terms of its displacement from an initial position. For the displacement along the *x* direction:

$$G_s(x,\tau) = \left\langle \delta\left[x - x_i(t+\tau) + x_i(t) \right] \right\rangle \qquad (7)$$

and similarly for the *y* and *z* directions. These directions are statistically equivalent in an isotropic system. The top panel of

Fig. 8 shows the Van Hove self-correlation functions of Li^+, obtained at different correlation times (τ = 0.01, 0.1, and 1 ns).

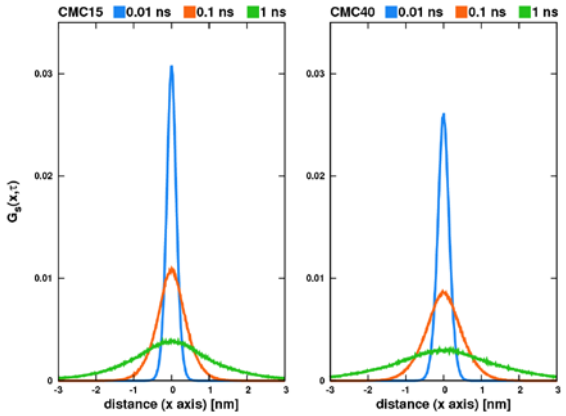

Fig. 8. Van Hove self-correlation functions for Li^+ in CMC15 (left) and CMC40 (right), at τ = 0.01, 0.1, and 1 ns.

In both CMC15 and CMC40, all distributions are characterized by a single peak with Gaussian-like profile. The extent of the deviations from it can be quantified by the non-Gaussianity parameter α_2, defined as[35]:

$$\alpha_2 = \frac{\langle \Delta x^4 \rangle}{3\langle \Delta x^2 \rangle^2} - 1 \qquad (8)$$

In general, this is time-dependent, but in our cases we observe roughly constant values, with $\alpha_2 \cong 0.2\text{-}0.3$ between 1 and 25 ns. Positive α_2 values indicate a larger "tail" in the displacements distribution. However, these are small in comparison to those of other systems characterized by slow, non-Gaussian diffusion, such as some ionic liquids, colloidal fluids and glassy systems.[36] Hence, the Li^+ motions appears to be essentially Gaussian and diffusive, much like in simple aqueous solutions. This conclusion agrees with the α=1.00 exponent obtained from the NMR measurements (see Eq. (2) and Figure 2b). This is remarkable, considering that the simulations and the experiments cover two widely different time scales (roughly 10^{-8} s and 10^{-1} s, respectively). On the other hand, there are several important counter-examples to this behavior, with Li+ undergoing sub-diffusive motion up to relatively long times (tens of ns's) in poly(ethyleneoxide)[37] and in ionic liquids[38]. In these cases, the crossover time from sub-diffusive to diffusive behavior was shown to correlate with the inverse of the frequency of some characteristic hopping events.

To further investigate the effect of carboxyl coordination on Li^+ diffusion, we calculated separate Van Hove distributions for coordinated (e.g. within the cutoff R=0.256 nm from a carboxyl oxygen, at τ=0 ns) and non-coordinated Li^+. The results are shown in the bottom panel of Fig. 9 for the shortest correlation time (τ=0.01 ns). Also in this case, the distributions show similar, nearly Gaussian profiles. The absence of secondary peaks allows us to exclude significant discrete "hopping" motion for Li^+, between different coordination environments.

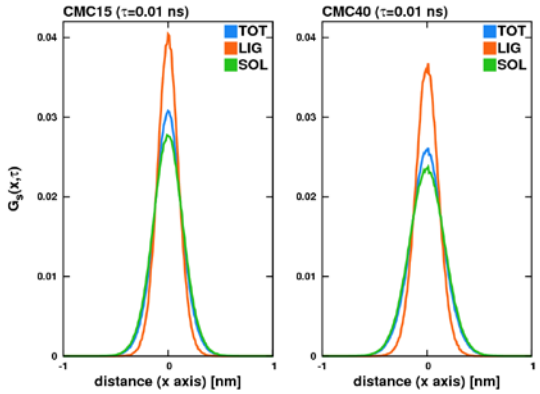

Fig. 9. Partial self-correlation functions for Li^+ in CMC15 and CMC40 at τ = 10 ps, for initially carboxy-coordinated (LIG) and free Li^+ ions (SOL).

To estimate the diffusion coefficients for "bound" (LIG) and "free" (SOL) Li^+ ions, the distributions were fitted according to a one-dimensional Gaussian with variance $\langle x^2 \rangle = 2D\tau$:

$$G_s(x,\tau) = \frac{1}{(4\pi D\tau)^{1/2}} e^{-\frac{x^2}{4D\tau}} \qquad (9)$$

The resulting diffusion coefficients are (in cm^2/s): $D_{LIG}=0.72\times10^{-5}$ and $D_{SOL}=0.86\times10^{-5}$ in CMC15, $D_{,LIG}=0.75\times10^{-5}$ and $D_{SOL}=0.94\times10^{-5}$ in CMC40. These estimates are consistent the values already given in Table 1. As expected, the Li^+ ions directly interacting with CMC diffuse slower than those in solution. However, their similarity indicates that the exchange between these "states" of the ions is quite fast. This is confirmed by the average residence times of Li^+ on a CMC monomer, calculated using the same cutoff distance as before (R=0.256 nm). The results are 0.68±0.72 ns and 1.1±1.4 ns for CMC15 and CMC40, respectively. Despite of the large standard deviations in these estimates, which are due to the high variability in residence times, we may conclude that attachment-detachment dynamics of the ions occurs on the nanosecond time scale.

Conclusions

We have investigated the diffusion of Li^+ in CMC-based solutions and gels, at polymer and salt concentrations similar to those tha may be used in the electrolyte of environmentally friendly, aqueous Li-ion batteries. Our aim was to establish some background knowledge about the mechanism of lithium transport in aqueous polyelectrolyte systems, and to cross-validate the NMR and MD methods, which can be used to investigate them.

The variable-time PFGSE-NMR measurements demonstrate that Li^+ ions undergo nearly free diffusion also in the presence of CMC, despite of the high viscosity of these systems (they are solid-like gels at high CMC concentrations). Comparison of the NMR results on LiCl solutions, with and without CMC-Li, shows that the latter moderately decreases the Li^+ diffusion coefficient, with a maximum difference of about 14% for the most concentrated systems (i.e., SOL15 and CMC15). The linear dependence found in experimental signal decays provided a clear indication of unrestricted Gaussian diffusion. In

order to make the atomistic MD simulations affordable, the systems investigated by them were necessarily simplified. Nonetheless, despite the differences in oligomer length and degree of substitution, the MD simulations provided Li^+ diffusion coefficients in very good agreement with the experimental ones.

In order to rationalize the effect of CMC on Li^+ diffusion, we have analyzed the distribution of distances associated with various atom types. We have found that Li^+ interacts strongly and selectively with the oxygen atoms of the carboxylate groups, giving rise to a rich variety of coordination patterns. Nonetheless, this does not slow down appreciably the Li^+ diffusion, and our simulations show no evidence of "hopping" between different binding sites. Rather, the dynamics is characterized by a fast exchange of Li^+ between CMC and the aqueous environment, which occurs on the nanosecond time-scale.

Experimental Section

NMR experiments. Three stock solutions of LiCl 0.42 M (SOL40), 0.72 M and 1.0 M (SOL15) in water-D_2O were initially. Samples with different concentrations of CMC in LiCl solution (CMC40, CMC25 and CMC15, respectively 1:40, 1:25 and 1:15 w:w) were prepared from these, by adding and dissolving the defined amount of CMC-Na (WALOCEL™ CRT 2000 PA by DowWolff Cellolosics, degree of substitution DS=0.82-0.95, Brookfield viscosity 1.9-2.8 Pa·s). The mixtures were stirred for a few minutes in order to obtain clear solutions, which had a gel-like consistency. The samples (0.5-1.0 g) were transferred in a 5 mm high resolution NMR tube. We performed ^{7}Li PFGSE experiments on a Bruker DRX 500 spectrometer equipped with a broadband probe, using the bipolar pulse longitudinal eddy current delay (BPPLED) pulse sequence[34]. The experimental parameters such as the duration of the magnetic field pulse gradients (δ) and the diffusion times (Δ) were optimized for each sample in order to obtain complete dephasing of the signals with the maximum gradient strength. For the investigated samples, δ values were in the range 1.5-3 ms while the Δ values were 100-300 ms. Several experiments were carried out with different δ-Δ pairs, in order to study the type of motion for the two CMC-Li/LiCl solutions. In each PGSE experiment, a series of 32 spectra with 16K points were collected. The pulse gradients were incremented from 2 to 95% of the maximum value in a linear ramp.

MD simulations. We have simulated the dynamics of CMC-Li oligomers made up of 10 monomers. A schematic representation of the monomer is given in Fig. 1.Molecular models of CMC-Li suitable for MD simulations were prepared starting from cellulose oligomers containing 10 β-D-glucopyranose units. All hydrogen atoms bound to O6 atoms were replaced by lithium-carboxymethyl groups. Thus our CMC model has a DS=1, and the functionalization is exclusively at the O6 position, which is known to be most reactive one towards carboxymethylation. Oligomer chains were capped at both ends (C1 and C4, respectively) by methoxy groups. An atomistic all-atom force field for CMC was developed exploiting the CHARMM force field parameters for carbohydrate derivatives[39]. Also the Li+ parameters were taken from CHARMM, and we used the TIP3P model for water[40].

Table 4. Composition (no. of molecules or ions) of the simulated systems. CMC^{10-} indicates the CMC decamers.

System	CMC^{10-}	Li^+	Cl^-	H_2O
SOL40	—	240	240	31805
SOL15	—	240	240	11270
CMC40	6	300	240	31805
CMC25	6	300	240	18773
CMC15	6	300	240	11270

Simulation boxes containing six CMC-Li oligomers in aqueous LiCl solutions were prepared and equilibrated. The starting box size was adjusted to simulate systems with CMC concentrations identical to the experimental ones (1:15, 1:25 and 1:40 w:w, corresponding to CMC15, CMC25 and CMC40). In addition to the 60 Li+ counterions which neutralize the charge of the CMC oligomers and the appropriate number of water molecules, we added 240 Li^+ and 240 Cl^- ions. These correspond to LiCl concentrations of 1.0 mol/L and 0.42 mol/L, respectively for CMC15 and CMC40. Two additional input files (SOL40 and SOL15) were prepared by removing the CMC-Li oligomers from CMC40 and CMC15 and were used for the simulation of Li^+ diffusion in water. The composition of all the simulated systems is summarized in Table 4.

All simulations were performed with the GROMACS5 molecular dynamics simulation package.[41] The equations of motion were integrated with a 1 fs timestep, with no restraints to bond lengths or angles. Periodic boundary conditions were applied along all axes, using cubic simulation boxes as appropriate for an isotropic system. Short-range non-bonded interactions, which are modelled in CHARMM by Lennard-Jones potentials, were truncated and shifted to zero at R_{cutoff}=1.2 nm. Instead, long-range electrostatic interactions were treated by the Particle-Mesh-Ewald method[42] with a Fourier grid spacing of 0.12 nm. All systems were first equilibrated at constant temperature (300 K) and pressure (1 bar) for 10 ns, in order to adjust the box size and reach the correct the density. Temperature and pressure were controlled by the Berendsen methods[43], with relaxation times τ_T=0.1 ps and τ_P=1.0 ps. Afterwards, 50-ns production runs were performed at constant temperature and density. The resulting trajectories were then processed to extract relevant structural and dynamical properties. Pairwise radial distribution functions, coordination numbers and diffusion coefficients were calculated using the tools provided within GROMACS. In-house programs were specifically developed to analyze the distribution and coordination of Li^+ cations around the CMC molecules.

Acknowledgements

The authors thank the European Commission for the financial support within the FP7 Project GREENLION (Grant agreement no. 285268).

Keywords: NMR Spectroscopy • Diffusion • MD Simulations • Aqueous Li-ion batteries • Natural polyelectrolytes

[1] M. S. Whittingham, *Proc. IEEE* **2012**, *100*, 1518-1534.
[2] M. Winter, R. J. Brodd, *Chem. Rev*. **2004**, *104*, 4245–4270.
[3] M. Armand, J. M. Tarascon, *Nature* **2008**, *451*, 652-657.
[4] H. D. Abruña, Y. Kiya, J. C. Henderson, *Phys. Today* **2008**, December issue, 43-47.
[5] B. Dunn, H. Kamath, J.-M. Tarascon, *Science* **2011**, .
[6] B. Scrosati, J. Hassoun, Y.-K. Su, *Energy Environ. Sci.* **2011**, *4*, 3287-3295.
[7] K. Kang, Y. S. Meng, J. Bréger, C. P. Grey, G. Ceder, *Science* **2006**, *311*, 977-980.
[8] Y. Hu, X. Sun, *J. Mater. Chem. A*, **2014**, *2*, 10712-10738.
[9] B. Scrosati, J. Garche, *J. of Power Sources* **2010**, *195,* 2419-2430.
[10] P.G. Balakrishnan, R. Ramesh, T. Prem Kumar, *J. of Power Sources* **2006**, *155,* 401–414.
[11] M. S. Whittingham, *Chem. Rev*. **2014**, *114*, 11414–11443.
[12] M. N. Obrovac and V. L. Chevrier, *Chem. Rev*. **2014**, *114*, 11444-11502.
[13] B. Lestriez, *C. R. Chimie* **2010,** *13*, 1341-1350.

[14] M. Park, X. Zhang, M. Chung, G. B. Less, A. M. Sastry, *J. of Power Sources* **2010**, *195*, 7904–7929.

[15] K. Xu*, Chem. Rev*. **2014**, *114*, 11503–11618.

[16] F. Beck, P. Rüetschi, *Electrochim. Acta* **2000**, *45*, 2467-2482.

[17] H. Kim, J. Hong, K.-Y. Park, H. Kim, S.-W. Kim, and K. Kang, *Chem. Rev*. **2014**, *114*, 11788-11827.

[18] L. Wu, J. R. Dahn, D. S. Wainwright, *Science* **1994**, *264*, 1115-1118.

[19] S. F. Lux, L. Terborg, O. Hachmöller, T. Placke, U.-W. Meyer, S. Passerini, M. Winter, S. Nowak, *J. Electrochem. Soc.* **2013**, *160*, A1694-A1700.

[20] J. Drofenik, M. Gaberscek, R. Dominko, F. W. Poulsen, M. Mogensen, S. Pejovnik, J. Jamnik, *Electrochim. Acta* **2003**, *48*, 883-889.

[21] F. M. Courtel, S. Niketic, D. Duguay, Y. Abu-Lebdeh, I. J. Davidson, *J. Power Sources* **2011**, *196*, 2128-2134.

[22] Y. S. Zhu, S. Y. Xiao, M. X. Li, Z. Chang, F. X. Wang, J. Gao, Y. P. Wu, *J. Power Sources* **2015**, *288*, 368-375.

[23] J. Song, M. Zhou, R. Yi, T. Xu, M. L. Gordin, D. Tang, Z. Yu, M. Regula, and D. Wang, *Adv. Funct. Mater.* **2014**, *24*, 5904–5910.

[24] L. Zhang, Z. Liu, G. Cui, L. Chen, *Prog. Polym Sci.* **2015**, *43*, 136-164.

[25] N. Alias, A. A. Mohamad, *J. Power Sources* **2015**, *274*, 237-251.

[26] K. Kenji, Elsevier, Amsterdam, The Netherlands, First Edition, **2005**.

[27] M. Mancini, F. Nobili, R. Tossici, R. Marassi, *Electrochim. Acta* **2012**, *85*, 566-571.

[28] M. Cerbelaud, B. Lestriez, R. Ferrando, A. Videcoq, M. Richard-Plouet, M. T. Caldes, D. Guyomard, *Langmuir* **2014**, *30*, 2660−2669.

[29] a) L. Qiu, Z. Shao, D. Wang, F. Wang, W. Wang, J. Wang, *Carbohydrate Polymers* **2014**, *112*, 532-538; b) N. Loeffler, J. von Zamory, N. Laszczynski, I. Doberdo, G.-T. Kim, S. Passerini, Journal *of Power Sources* **2014**, *248*, 915-922; c) K. A. Seid, J. C. Badot, O. Dubrunfaut, S. Levasseur, D. Guyomarda, B. Lestriez*, J. Mater. Chem*. **2012**, *22*, 24057- 24066.

[30] L. Qiu, Z. Shao, W. Wang, F. Wang, D. Wang, Z. Zhou, P. Xiang, C. Xu, *RSC Adv*. **2014**, *4*, 24859-24862.

[31] a) M. Abrami, I. D' Agostino, G. Milcovich, S. Fiorentino, R. Farra, F. Asaro, R. Lapasin, G. Grassi, M. Grassi, *Soft Matter* **2014**, *10*, 729–737; b) M. Ferro, F. Castiglione, C. Punta, L. Melone, W. Panzeri, B. Rossi, F. Trotta, and A. Mele *Beilstein J. Org. Chem*. **2014**, *10*, 2580-2593.

[32] J. Kärger, *Chem. Phys. Chem.* **2015**, *16*, 24-51.

[33] a) M. Mandel, Physical properties of polyelectrolyte solutions – An introduction, AIM, Pisa, 1999; b) R. R. Netz and D. Andelman *Physics Reports* **2003**, *380*, 1-95; c) A. Yu. Grosberg, T. T. Nguyen, and B. I. Shklovskii *Rev. Mod. Phys*. **2002**, *74*, 329-345.

[34] a) L. Van Hove, *Phys. Rev*. **1954**, *95*, 249-262; b) A. Rahman, *Phys. Rev*. **1964**, *136*, A405-A411; c) J.-P. Boon and S. Yip, Molecular Hydrodynamics, Dover Publications, New York, 1991.

[35] a) B. Wang, J. Kuo, S. C. Bae, S. Granick, *Nature Materials* **2012**, 11, 481-485; b) Z. Ho, C. J. Margulis, *Acc. Chem. Res.* **2007,** *40,* 1097–1105; c) G. D. G. Phillies, *Soft Matter* **2015**, *11*, 580-586.

[36] D. Wu, A. Chen, C. S. Johnson Jr, *J. Magn. Reson., Ser. A*, **1995**, *115*, 260-264.

[37] O. Borodin, G. D. Smith, *Macromolecules* **2006**, *39*, 1620-1629.

[38] O. Borodin, G. D. Smith, W. Henderson, *J. Phys. Chem. B* **2006**, *110*, 16879-16886.

[39] a) O. Guvench, S. N. Greene, G. Kamath, J. W. Brady, R. M. Venable, R.W. Pastor, A.D. Jr. MacKerell *J. Comput. Chem*. **2008,** *29*, 2543-2564; b) S. S. Mallajosyula, and A. D. Jr. MacKerell *J. Phys. Chem. B* **2011**, *115*, 11215-11229.

[40] W.L. Jorgensen, J. Chandrasekhar; J. D. Madura, R. W. Impey, M. L. Klein, *J. Chem. Phys*. **1983**, *79*, 926.

[41] a) D. van der Spoel, E. Lindahl, B. Hess, G. Groenhof, A. E. Mark, and H. J. C. Berendsen, *J. Comp. Chem*. **2005** *26*, 1701-1718; b) B. Hess, C. Kutzner, D. van der Spoel, and E. Lindahl *J. Chem. Theory Comp.* **2008**, 4, 435-447.

[42] Darden, T.; York, D.; Pedersen, L. *J. Chem. Phys*. **1993**, *98*, 10089-10092.

[43] H. J. C. Berendsen, J. P. M. Postma, W. F. van Gunsteren, A. DiNola, J. R. Haak, *J. Chem. Phys*. **1984**, *81*, 3684-3690.

Entry for the Table of Contents

FULL PAPER

Aqueous lithium-ion batteries are getting into the focus because they promise to combine high energy and environmental friendliness. This requires, among other things, the development of aqueous electrolytes. In this manuscript, the Li^+ cation coordination and dynamics in the gel-like electrolyte made with Li-carboxymethyl cellulose are investigated by NMR and MD simulations.

*M. Casalegno, F. Castiglione, M. Passarello, A. Mele, S. Passerini and G. Raos**

Page No. – Page No.

Association and diffusion of Li^+ in carboxymethylcellulose solutions with application to environmentally friendly Li-ion batteries: a combined Molecular Dynamics and NMR study